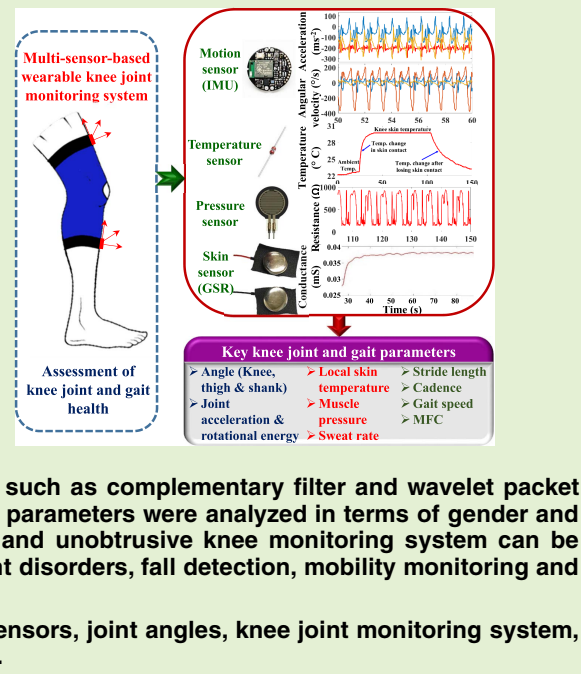
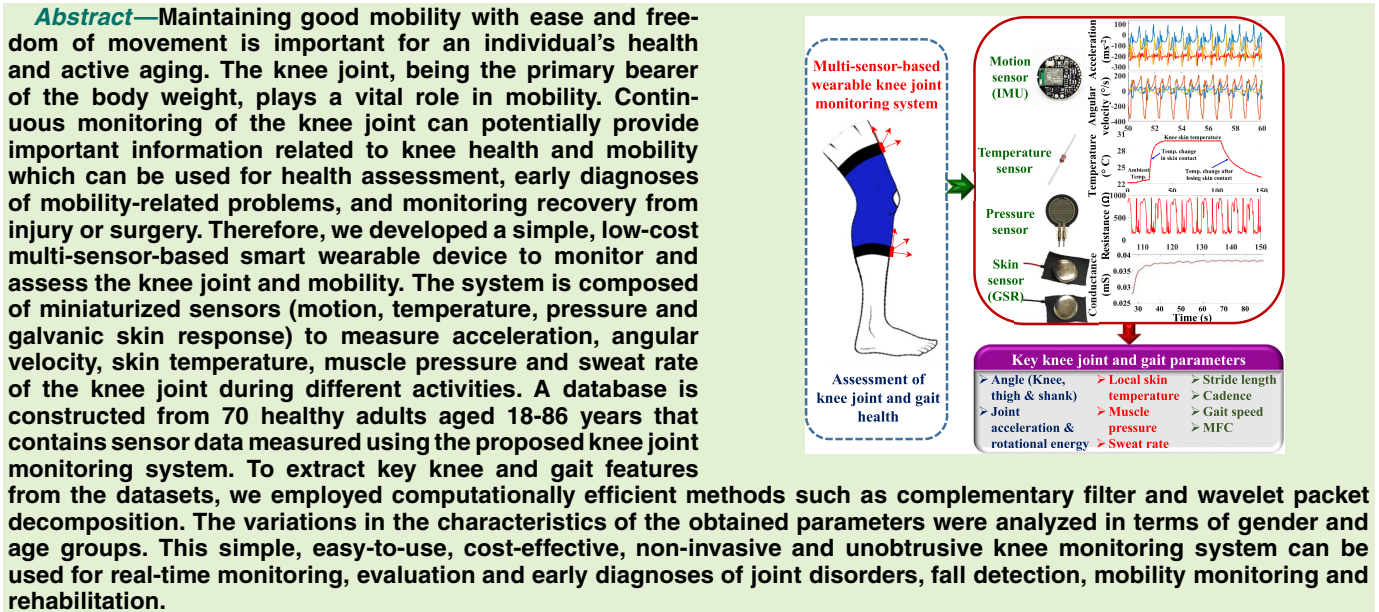


A Simple, Low-Cost Multi-Sensor-Based Smart Wearable Knee Monitoring System

Abu Ilius Faisal, Sumit Majumder^{ID}, Graduate Student Member, IEEE, Ryan Scott^{ID}, Tapas Mondal, David Cowan, and M. Jamal Deen^{ID}, Life Fellow, IEEE



I. INTRODUCTION

THE rapidly aging population is expected to cause increased socio-economic burden on many societies all over the world in terms of healthcare and welfare [1]. One

Manuscript received December 6, 2020; accepted December 8, 2020. Date of publication December 14, 2020; date of current version February 17, 2021. This work was supported in part by the Canada Research Chair program, in part by the AGE-WELL Catalyst Funding Program of the McMaster Institute for Research on Aging (MIRA), and in part by the Natural Sciences and Engineering Research Council (NSERC) of Canada. The associate editor coordinating the review of this article and approving it for publication was Prof. Kazuaki Sawada. (*Corresponding author: M. Jamal Deen.*)

Abu Ilius Faisal, Sumit Majumder, Ryan Scott, and M. Jamal Deen are with the Department of Electrical and Computer Engineering, McMaster University, Hamilton, ON L8S 4K1, Canada (e-mail: faisaa4@mcmaster.ca; majums3@mcmaster.ca; scottr8@mcmaster.ca; jamal@mcmaster.ca).

Tapas Mondal is with the Faculty of Health Science, McMaster University, Hamilton, ON L8S 4K1, Canada, and also with the Department of Pediatrics, McMaster University, Hamilton, ON L8S 4K1, Canada (e-mail: mondalt@mcmaster.ca).

David Cowan is with the Department of Medicine, St. Joseph's Healthcare Hamilton, Hamilton, ON L8N 4A6, Canada (e-mail: cowand@mcmaster.ca).

Digital Object Identifier 10.1109/JSEN.2020.3044784

of the major health concerns among the older adults is the loss of mobility that has significant social, mental and physical consequences [2]. Aging, coupled with common chronic diseases such as arthritis or diabetes, often results in restricted mobility [2]. In addition, it results in accelerated sarcopenia in older adults which in turn increases the risk of falls and fractures [3], [4]. With the aging population, the cost of services provided by support workers for daily personal care, and the cost of direct treatment and hospitalization for the musculoskeletal disorders in older people has become a significant financial/social burden on governments, society and family members [5]–[7]. A major component of this high cost can be reduced by implementing predictive and preventive solutions in wearable platforms, thus enabling long-term and in-home monitoring of elderly's musculoskeletal-related health issues and injuries [8], [9].

Monitoring and assessing the mechanical and physiological characteristics of the key joints during normal daily activities may provide valuable insights about the initiation and development of different musculoskeletal disorders. Among all the joints, the knee is the most critical joint in the human body for

mobility [10]. Knee joints bear most of the body-weight and are highly susceptible to injury due to repetitive use and other factors such as genetics, obesity, occupation and sports [10], [11]. Its proper function is essential for good mobility and is considered as one of the most important and critical health assessment parameters.

A low-power and easy-to-use wearable device for knee joint monitoring can have the advantage of providing long term observations and records of parameters related to knee health and mobility without restricting people to a hospital or a laboratory, and without hindering their normal daily activities [12]–[17]. The recorded data can further be utilized and interpreted by medical personnel for clinical diagnosis and treatment of knee joint and mobility-related problems. Also, by comparing the measured knee parameters of an individual person with the reference values, early diagnosis of mobility-related problems becomes feasible [12]. Thus, a wearable knee-joint monitoring device can be used for an extensive range of mobility-related applications such as rehabilitation, sports medicine, human activity assessment and virtual guided training [12].

The objective of this research is to develop a wearable and low-cost smart knee monitoring device. Therefore, we investigated different sensing technologies and designed our wearable monitoring system by fusing data from multiple types of sensors (IMU – inertial measurement unit, temperature, pressure, and GSR – galvanic skin response). The IMU sensors provide mechanical parameters such as knee angle, motion and orientation by measuring rotation and acceleration. The system also includes sensors to record and monitor other important parameters such as knee skin temperature, skin conductance and muscle pressure around the knee joint. All sensors used in this system are low-cost, low-power, small and lightweight. We used an Android smartphone app to gather and store the sensors' data wirelessly and later applied efficient signal analysis and data processing techniques for extracting key joint and gait-related features for knee health and mobility analysis. Thus, the proposed system (Fig. 1) is suitable for real-time monitoring of knee joints with limited processing resources and is capable of providing useful information about the knee health of an individual.

A brief overview of related works and different approaches of knee monitoring is presented in Section II. In Section III, the details of the proposed system design, experimental protocol and data acquisition methods are described. The processing and analysis techniques of the collected data are demonstrated in Section IV. This is followed by the presentation and discussion of results in Section V. Finally, in Section VI, we conclude the manuscript by summarizing the work and describing some future research possibilities.

II. RELATED WORKS

At present, most of the clinically used joint monitoring systems are based on goniometers [18]–[21] or video/imaging systems [22]–[24]. The traditional goniometer-based systems usually use resistive potentiometers or strain gauges for joint monitoring. However, inflexibility and low accuracy are the major drawbacks of such systems. To overcome these

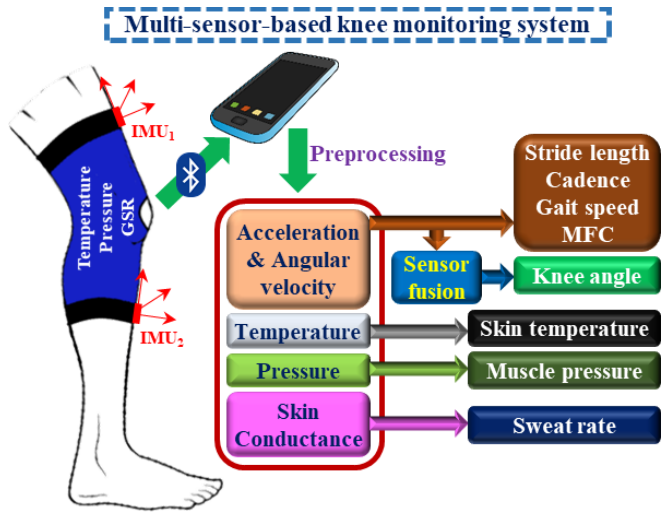


Fig. 1. Proposed multi-sensor-based wearable knee joint monitoring system.

disadvantages, some researchers developed flexible optical fiber-based goniometers to measure joint parameters [25]–[27]. They measured changes in the attenuation of the transmitted optical signal through the optical fiber sensors placed on the knee joint to estimate the knee movements.

On the other hand, video/imaging-based knee monitoring systems rely on cameras and image processing techniques [22]–[24]. These systems provide quantitative measurement of joint positions and movements. However, they use complicated image processing algorithms and machine learning techniques to track joints and analyze mobility. Therefore, a complex and expensive setup with sophisticated image analysis tools is required for such systems. Moreover, these systems require a pre-equipped lab environment, which are not only expensive but also restrict the users in a limited space within the field of views of the cameras. Therefore, camera-based systems are not suitable for continuous and long-term monitoring of knee joints during daily activities.

Textile-based sensors such as flexible conductive wire sensors [28], flex sensors [29], [30] or strain sensors [31], [32] are also becoming popular for developing wearable knee joint monitoring systems due to their simple working principle. The pressure generated due to joint movement causes the resistance across the sensor to change that is directly related to the corresponding joint angles [29]. These sensors are usually stitched to flexible, skin-tight garments across the joint. However, these types of sensors are not suitable to monitor joint motion or orientation as most of them can only measure the single-axis movement.

Compared to other sensor technologies, inertial measurement unit (IMU) sensors are the most promising sensor unit for developing a wearable knee joint monitoring system, because of their compact size and capability of measuring joint parameters with precision and accuracy [33]–[35]. An IMU-based system can quantify joint motion and orientation by measuring the three-dimensional linear acceleration (accelerometer), angular velocity (gyroscope) and magnetic field vector (magnetometer) during joint movements. Most of the IMU-based systems used two calibrated IMUs placed

TABLE I
LIST OF DIFFERENT JOINT MONITORING SYSTEMS, AND THEIR ADVANTAGES AND LIMITATIONS

Types of Sensor	Human Joint	Parameter	Advantages	Limitations
[18]–[21] Electrogoniometer	Knee, ankle	Resistance / Strain	1. Based on resistive potentiometers or strain gauges application 2. Straightforward measurement	1. Large size, imprecision and fixed center configuration 2. High cost (hardware and software sold separately)
[22]–[24] Video/Imaging-based systems	Knee, hip, elbow, shoulder	Visual data	1. Able to detect movements of multiple joints simultaneously 2. No body-worn sensors are needed	1. Limited coverage area 1. Complex method with expensive setup and sophisticated analyses
[25]–[27] Optical fiber sensors	Knee, elbow	Optical navigation and Signal attenuation	1. High resolution, high reaction speed, flexibility and lightweight 2. Immunity to electromagnetic interference	2. Limited measurement range and 3D motion tracking may not be possible 2. Sensitive to temperature and humidity as well as placement location
[28]–[32] Textile-based sensors	Knee, hip, elbow, fingers	Resistance / Strain	1. Low-cost, flexible and suitable for long-term monitoring 2. Simple mechanism and easy integration with comfortable garments	1. Nonlinearity, low accuracy and ineligible to detect 3D movement 2. Performance degradation due to large mechanical strains and rigorous deformations
[37] Acoustic sensors	Knee	High-frequency soundwave	1. Lightweight and easily attachable around joints 2. Wireless monitoring is possible	1. Significant background and interface noise 2. Nonlinearity and low accuracy
[33]–[36] IMU sensors (accelerometer, gyroscope and magnetometer)	Knee, hip, elbow, shoulder	Linear acceleration, angular velocity and magnetic field vector	1. Low-cost, lightweight, compact, high accuracy and easy to install 2. Reliable for 3D joint movement and orientation detection	1. Signal drift 2. Sensors alignment is required in a multiple IMUs-based system
Our System IMU sensors (accelerometer, gyroscope and magnetometer), temperature, pressure and GSR sensors	Knee	Linear acceleration, angular velocity, local skin temperature, muscle pressure and sweat rate of knee joint skin	1. Low-cost, lightweight, compact, high accuracy and easy to install 2. Reliable for 3D joint movement and orientation detection 3. Capable of measuring other important physiological joint parameters (local skin temperature, sweat rate and muscle pressure) 4. Sensor fusion methods are applied to overcome signal drifts and alignment issues	1. Data analysis accuracy can be enhanced with a larger balanced dataset. 2. A stand-alone smart program is required for data acquisition, analysis and real-time feedback applications.

below and above a joint to measure data for calculating joint angle and orientation [33]–[36]. Apart from measuring the joint angle, an IMU-based system is also capable of measuring other important gait parameters such as stride length, minimum foot clearance (MFC), gait speed and cadence (steps per minute) [33] which are useful for gait analysis. Most commercially available IMU boards come with an integrated wireless module and built-in algorithms that make them convenient to develop a smart wearable device for continuous joint monitoring and gait analysis [14], [15], [33].

Therefore, we have adopted the IMU-based method and included additional relevant sensors (temperature, pressure and GSR) to develop a simple, efficient and low-cost wearable knee monitoring device. This system can provide information related to joint angle and motion, as well as measure other important physiological parameters such as local skin temperature, muscle pressure and sweat rate of the joint skin that are related to joint health. The information from different sensors can further be fused to deliver valuable information and assessment related to knee joint health. A comparison among our developed system and several published knee monitoring systems is presented in Table I.

III. SYSTEM DESIGN AND METHODOLOGIES

A. Sensors

Our smart knee monitoring system consists of a set of different miniaturized sensors wirelessly connected to a smart computing device with a real-time software program to record and process knee joint and mobility-related parameters. Our knee monitoring system includes sensors:

1) IMU Sensors: We selected the MetaWear CPro IMU from MbientLab Inc. for our system because of its small size, low-cost, good energy efficiency and low-power wireless connectivity. The IMU has dimensions of 24 mm diameter × 6 mm thick and it is powered by a replaceable coin-cell battery (200 mAH). The IMU can continuously stream or log data for upto 48 hours and the sleep mode supports 6 months idle time. Moreover, the newer version of the sensor (MetaMotionR) comes with a rechargeable Lipo battery which makes it more convenient for continuous monitoring. The technical specifications of the CPro IMU are presented in Table II. We used the accelerometer and gyroscope data collected from two IMUs to monitor the movements of a knee joint. The accelerometer and the gyroscope have full-scale ranges of $\pm 16g$ and $\pm 2000^{\circ}/s$, respectively, and can acquire signal at a sample rate of 100 Hz. The MetaWear CPro is also equipped with general-purpose input/output (GPIO) pins which can be used to connect additional sensors to the board. Hence, we used another CPro to connect another three sensors described below using the GPIO pins and to collect their data.

2) Temperature Sensor: A 135-104LAG-J01 discrete thermistor (NTC) from Honeywell Sensing and Productivity Solutions was used to measure the knee skin temperature. This is a high-quality glass-encapsulated unit of 100,000 Ohm resistance with $\pm 10.0\%$ tolerance and $25/85 \text{ BETA} = 3974$. The technical specifications of the temperature sensor are presented in Table II.

3) Pressure Sensor: A force sensitive resistor (FSR® 402 Short) from Interlink Electronics was used to measure the

TABLE II
TECHNICAL SPECIFICATIONS OF SENSORS

Sensor Parameters		Value
MetaWear CPro IMU	Weight	Ultra-lightweight at just 0.2 oz
	Size	24 mm diameter x 6 mm thick
	Power consumption	Sleep mode supports 6 months idle time
	Power Source	200mAH coin-cell (CR2032) replaceable
	Synchronized timestamp	Supports multiple devices simultaneously
	Data Transfer	Bluetooth Low Energy Smart®
	Range	$\pm 2, \pm 4, \pm 8, \pm 16$ g \rightarrow Accelerometer $\pm 125, \pm 250, \pm 500, \pm 1000, \pm 2000$ /s \rightarrow Gyroscope
	Resolution	16bit
	Sample Rate	0.001Hz – 100Hz
	Weight	Ultra-lightweight at just 0.2 oz
135-104LAG-J01 discrete thermistor	Size	24 mm diameter x 6 mm thick
	Power consumption	Sleep mode supports 6 months idle time
	Resistance at 25°C	100,000 Ohm
	Resistance tolerance	$\pm 10.0\%$
FSR® 402 Short	Operating Temperature	-60 °C to 300 °C [-76 °F to 572 °F]
	Size	2.0 mm diameter, 28.6 mm lead length
	Beta	3974
	Actuation Force	0.1 Newtons
	Force Sensitivity Range	0.1 - 10.02 Newtons
	Force Repeatability	$\pm 2\%$ (single part) and $\pm 6\%$ (part to part)
	Non-Actuated Resistance	10 MW
	Response Time	3 μ s
	Size	18.28mm diameter (active area 12.7mm diameter)
	Thickness Range	0.2 - 1.25 mm
GSR Sensor	Operating Temp. Range	-30 - +70 °C
	Actuation Force	0.1 Newtons

muscle pressure around the knee. It is a sensitive single-zone force sensing resistor that is circular in shape with a diameter of 18.28 mm. The diameter of its active area is 12.7mm. The sensor has a response time of 3 μ s. The resistance decreases with the increasing force applied to the surface of the sensor. The technical specifications and device characteristics of the force sensor are presented in Table II.

4) GSR Sensor: A two-electrodes-based GSR sensor was used for the measurement of local skin sweat gland activity (skin conductance) that is related to skin stress and perspiration. The skin conductance increases as the sweat gland activity increases. The most common method to measure a GSR signal is based on applying a constant low voltage to two electrodes that are in contact with the skin and measuring the current. The circuit also contains a resistor in series that has very small resistance compared to the skin resistance. In this system, we used the CPro IMU board as the voltage source and connected two electrodes of the GSR sensor with the power supply and GPIO pins of the board. With this setup, any change in the current flow due to a change in the skin conductance can be detected.

B. Implementation of Knee Monitoring System

First, we built a combined sensing module with temperature, pressure and GSR sensors by connecting these sensors externally to a MetaWear CPro IMU board using its GPIO pins (Fig. 2(a)). Here, the CPro IMU board performs as the central processing unit and power supply which collects the

readings from all three sensors and transfers the data wirelessly into a smart device for further analysis. Then we attached this integrated sensing module on the inner side of an adjustable and comfortable textile-based knee brace and two additional IMUs with two Velcro straps. This system transfers data over Bluetooth to a smartphone or a portable computer where knee joint data from all sensors can be stored and further processed. A photograph of all the sensors and the prototype of our smart wearable knee joint monitoring system is presented in Fig. 2(b).

C. Data Acquisition System and Protocol

The developed knee monitoring system was worn around the knee joint with the sensors positioned at the frontal section. Prior to data acquisition, a letter of consent and the study protocol including some key information such as the motivation for the study, data acquisition procedure, and data security and privacy protocols were prepared, reviewed and approved by the University's Research Ethics Board. A total of 70 healthy adults (18 to 86 years) participated in this study. Each participant was requested to answer a questionnaire form prepared by a physician to collect some key physical information including sex, age, weight, height, leg length, and knee circumference. The subjects walked for approximately 200 meters on a well-illuminated, obstacle-free wide walkway at their preferred walking speed with the knee brace strapped around the knee joint. The two IMUs were positioned in such an orientation that the x, y and z-axis respectively point towards the upright (longitudinal), outward (mediolateral) and forward (anteroposterior) directions. To maintain the consistency of measurements among all subjects, the knee brace was always strapped in the same location and orientation, keeping the knee in the middle, and the IMUs at a distance of 14 cm below and above the knee joint (Fig. 2(b)). An Android app in the smartphone was capable of collecting data from multiple CPro modules at the same time over the Bluetooth platform, thus allowing for synchronous data collection from all the five sensors. Thus, our system is very suitable for gathering real-time knee data from a subject performing the experiment. All the sensors' data are anonymously stored in the computer in a readable file format (*.csv) which are then used for post-processing and further analysis.

IV. SIGNAL PROCESSING AND DATA ANALYSIS

The collected data from the knee monitoring system undergoes several signal preprocessing and data analysis steps to extract usable joint parameters and assess the mobility status of an individual. In this Section, we will discuss these signal processing and analysis techniques implemented for the collected data. Then, we determine the necessary knee joint and gait parameters such as knee angle, stride length, minimum foot clearance (MFC), gait speed, cadence (steps per minute), local skin temperature, skin conductance and the muscle pressure around the knee joint. We also extracted a set of energy spectral features related to knee joint movement from the preprocessed IMU signals (linear acceleration and angular velocity).

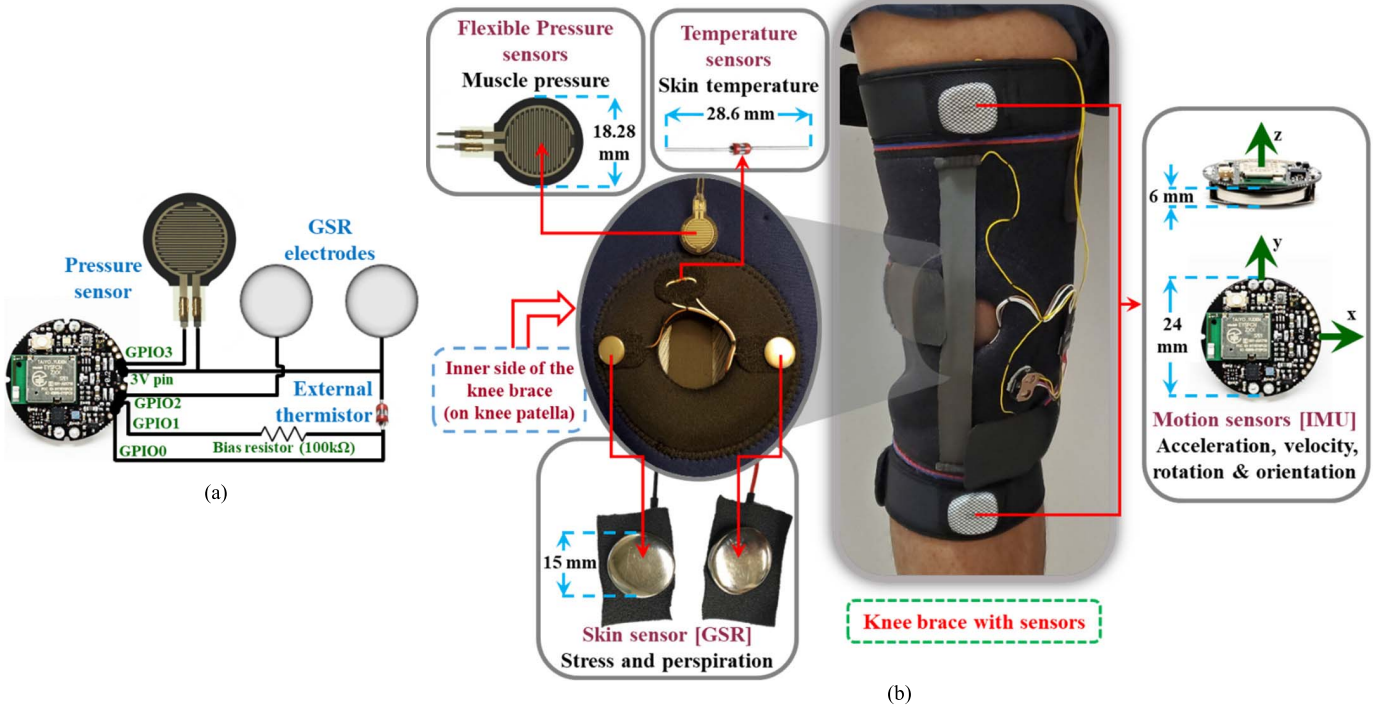


Fig. 2. (a) Integration of external sensors with CPro IMU board (b) Multi-sensor-based smart wearable wireless knee joint monitoring system.

A. Preprocessing

The raw data from the IMU include high-frequency noise from the vibration of the device and ambient environment which degrades the sensor readings, and in turn, affect its accuracy. To remove this high-frequency noise, the sensor data is filtered using a fifth-order digital low-pass Butterworth filter. Since most of the significant features of the knee joint motion signals remain in the low-frequency region, we set the filter's cut-off frequency at 12 Hz. Although both IMUs are calibrated to gather simultaneous data with a fixed sample rate (50 Hz), the total sample counts are not always the same (slightly different) for a longer set of data. This loss happens because the IMUs use Bluetooth Low Energy (BLE) connection for transferring the data and the sensors push out data faster than the devices exchange data through the BLE connection. However, the total timespans of data from both IMUs are equal. Therefore, we regenerated a time-array with an interval of 0.02 s ($1 / 50$ Hz) for the whole span and then resampled the filtered data from two IMUs with respect to this time-array to time-align the data with each other. This alignment procedure is necessary for precise knee angle and motion calculation.

B. Knee Angle Estimation

We used the calibrated time-aligned data from two IMUs (IMU_1 and IMU_2) to measure the knee flexion and extension angles (Fig. 3). This angle calculation allows for estimating the range of motion (ROM) of the knee joint that varies with sex, age, physical structure and daily activities [38]. First, we used the accelerometer and gyroscope data individually to calculate the knee angle. The calculation from the accelerometer's data provides more absolute angle information

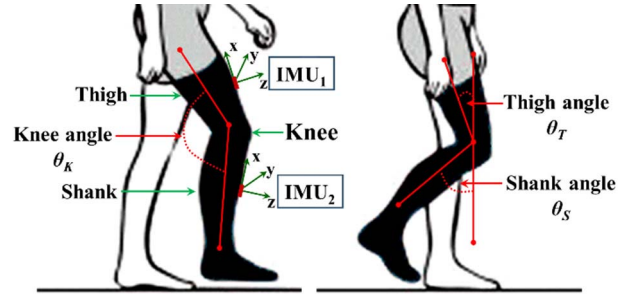


Fig. 3. Knee angle from IMU sensors.

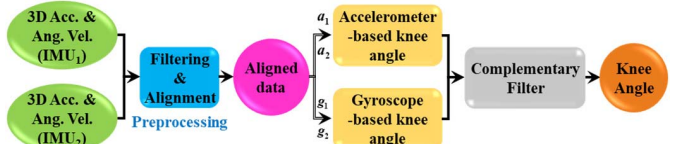


Fig. 4. Sensor fusion to calculate knee angle.

due to sensors' orientation independence from each other. However, the measurement accuracy can be affected by the high-frequency noise (mechanical) from the sensors' vibration, and the translational movement of the subject. On the other hand, it is simpler to calculate knee angles using the gyroscope data because its data is less impacted by high-frequency noise. However, the gyroscope data suffers from low-frequency drift over time. Therefore, we applied a fusion method (complementary filter) that combines both accelerometer and gyroscope data to remove accelerometer noise and overcome gyroscopic drift while computing the knee angle during walking (Fig. 4).

For extracting knee angles from the accelerometer readings while walking or during other activities, first, it is necessary to estimate the IMU's orientation vector on the shank and thigh

with respect to the Earth frame in a stationary position (straight standing with maximum knee extension). Second, we used the accelerometer readings while walking to compute the angle change between two vectors (stationary and walking) for both shank and thigh. The angle change from the accelerometer data was calculated using equation (1)

$$\theta_{acc} = \cos^{-1} \left(\frac{\vec{a}_{st} \cdot \vec{a}}{|\vec{a}_{st}| \cdot |\vec{a}|} \right), \quad (1)$$

where θ_{acc} is the angle between the two acceleration vectors, \vec{a}_{st} and \vec{a} . The vector in stationary position (different for thigh and shank) is \vec{a}_{st} , and the vector during walking is \vec{a} , whose value and direction changes with the sagittal movement of the thigh and shank. Thus, we can calculate the angle change for both thigh (θ_{Tacc}) and shank (θ_{Sacc}) while walking. We also determined the knee angle θ_{stacc} , in a stationary position from \vec{a}_{Tst} (thigh) and \vec{a}_{Sst} (shank) using the same equation. Then, the walking knee angle θ_{Kacc} , was calculated using equation (2)

$$\theta_{Kacc} = \theta_{stacc} - (\theta_{Tacc} + \theta_{Sacc}). \quad (2)$$

Calculation of the knee angle is performed using the angular velocities derived from two gyroscope data. The difference of the angular velocities around the joint axis was integrated with respect to time to calculate the angle. The knee angle θ_{Kgyr} , from the gyroscope data [35] is defined as:

$$\theta_{Kgyr}(t) = \int_0^t (g_1(\tau) \cdot j_1 - g_2(\tau) \cdot j_2) d\tau. \quad (3)$$

In equation (3), j_1 and j_2 represent the joint axes for IMU₁ and IMU₂, and g_1 and g_2 denote their respective gyroscope values.

The calculated angles from both accelerometer and gyroscope data are then combined, using sensor fusion, in a way such that the limitations of each sensor are mitigated. We used a complementary filter that is a simple method of implementing sensor fusion for the estimation of knee angle with a very low computational complexity [39]. Complementary filters have the effect of low-pass filtering the accelerometer data and high-pass filtering the gyroscope data, then combining them to give the result. Complementary filters can be implemented by using equation [39] (4)

$$\theta_K(t) = \alpha * \theta_{Kgyr}(t) + (1 - \alpha) (\theta_{Kacc}(t)), \quad (4)$$

where θ_K is the knee joint angle and α is the filter constant. It is a tunable parameter between 0 and 1 which determines the cut-off time for trusting the gyroscope and filtering in the accelerometer data. By selecting an appropriate time constant τ , for the filters, the value of α can be obtained from equation [39] (5)

$$\alpha = \frac{\tau}{(\tau + T_S)}. \quad (5)$$

In our work, we tried different cut-off times for the complementary filter to select the appropriate time constant, τ for achieving the highest accuracy. We obtained the optimal the value of α is 0.93 for a time constant (τ) of 0.25 s (4 Hz cut-off frequency) and sampling time (T_S) of 20 ms. This indicates

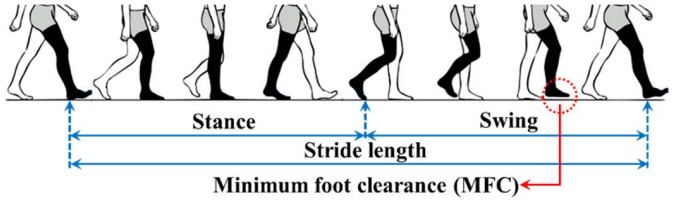


Fig. 5. Stride length and minimum foot clearance in one gait cycle.

that for time periods shorter than 0.25 s, the gyroscope data takes precedence and the accelerometer data is filtered out, while the accelerometer data takes precedence for time periods longer than 0.25 s.

C. Stride Length and Minimum Foot Clearance (MFC)

Stride length and minimum foot clearance (MFC) are two key parameters for knee joint functionality assessment as well as gait analysis [40], [41]. A short stride length and a low MFC are generally indicative of reduced knee joint movement and angle during walking. Stride length is calculated by measuring the distance covered in one stride cycle (Figs. 5 and 6) and MFC denotes the vertical distance of foot bottom/shoe sole above the ground during the mid-swing phase (shank is perpendicular and foot is parallel to the ground) of a gait cycle (Fig. 5). The movement of the foot during the mid-swing phase is considered as the most critical event while walking due to having the maximum horizontal velocity and minimum vertical distance above the ground [42]. Therefore, having a low MFC can trigger the possibility of trips and falls [43]. We utilized the gyroscope data from the shank's IMU to calculate the horizontal and vertical movement of the sensor during walking for stride length and MFC estimation. For these, we segmented the continuous motion signal into a series of stride cycles by applying a simple signal peak detection method where each cycle consists of one swing and one stance phase (Fig. 6).

To compute the displacement along the horizontal and vertical ground axes for each cycle, we first computed the shank angles both in the sagittal and transverse planes by integrating the gyroscope-measured angular velocities (equation (6))

$$\theta_S(t) = \int_0^t \omega(\tau) d\tau + \theta_S(0). \quad (6)$$

We also calculated the linear velocity v , by multiplying the angular velocity ω , with the radius r , of the angular rotation (equation (7))

$$v(t) = \omega(t) \times r. \quad (7)$$

In this case, the radius of the angular rotation r , is equal to the length from the knee to the bottom of the heel. We then resolved the calculated linear velocity v , into horizontal (v_{hor}) and vertical (v_{ver}) components with respect to the earth, according to equations (8) and (9)

$$v_{hor}(t) = v(t) \times \cos \theta_S(t), \quad (8)$$

$$v_{ver}(t) = v(t) \times \sin \theta_S(t). \quad (9)$$

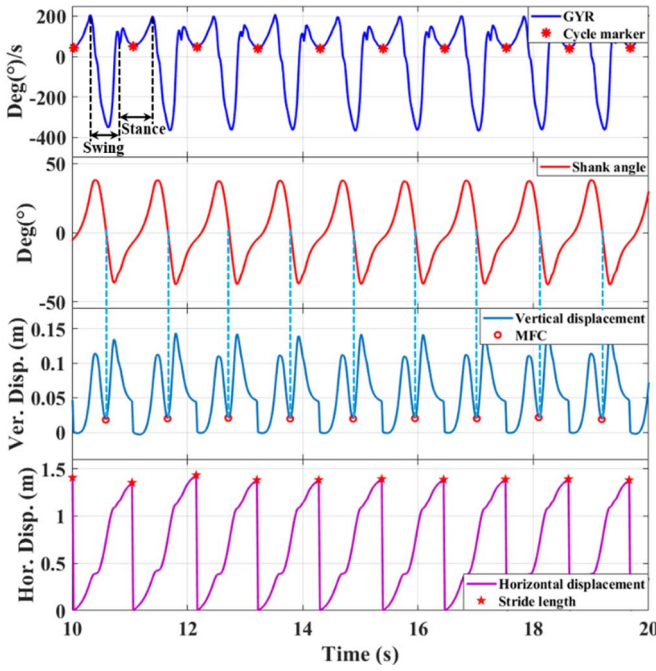


Fig. 6. MFC and stride length detection from vertical and horizontal displacement for each gait cycle.

While considering the horizontal velocity, the sensor has the movements both in sagittal and transverse planes. Therefore, for precise estimation, we calculated linear velocity components $v_{hor,s}$ and $v_{hor,t}$ in both of these two planes by using equation (8) and then used these two components to obtain the magnitude of horizontal gait velocity v_{gait} , (equation (10))

$$v_{gait}(t) = \sqrt{(v_{hor,s}(t))^2 + (v_{hor,t}(t))^2}. \quad (10)$$

A simple trapezoidal integration of the horizontal gait velocity v_{gait} , during one stride cycle from $t = 0$ to $t_{onecycle}$, provides the horizontal displacement also known as stride length (equation (11))

$$\text{Stride Length}(t) = \int_0^{t_{onecycle}} v_{gait}(\tau) d\tau. \quad (11)$$

Similarly, by integrating the vertical velocity v_{ver} , we obtained the vertical displacement s_{ver} (equation (12))

$$s_{ver} = \int_0^{t_{onecycle}} v_{ver}(\tau) d\tau. \quad (12)$$

The minimum foot clearance (MFC) occurs when the foot is parallel, and the shank is perpendicular to the ground. This means that the shank angle at the MFC is zero. Therefore, we used the calculated shank angle plot to identify the MFC location and then we determined the MFC in each stride cycle from the vertical displacement s_{ver} (Fig. 6).

D. Gait Speed and Cadence

We are also able to measure gait speed and cadence (steps per minute) using our system. These two gait parameters are commonly used to evaluate the overall performance of

walking [44]. To calculate the gait speed, the total distance of walking was divided by the travel time (equation (13)).

$$\text{Gait Speed} = \frac{D_{total}}{t_{stop} - t_{start}}, \quad (13)$$

where the total walking distance D_{total} , was calculated from the summation of stride lengths during each stride cycle from starting time t_{start} to stopping time t_{stop} (equation (14)).

$$D_{total} = \sum_{n=1}^N \text{Stride Length}. \quad (14)$$

In equation (14), N is the total number of gait cycles of an individual. We also used this number to calculate cadence using equation (15)

$$\text{Cadence} = \frac{N \times 2 \times 60}{t_{stop} - t_{start}}. \quad (15)$$

As each gait cycle consists of two steps, and cadence is expressed in steps per minute, hence in equation (15), N is first multiplied by 2 and 60, and then divided by travel duration to determine the cadence of an individual.

E. Temperature, Pressure and Skin Conductance

We measured the knee skin temperature, skin conductance and muscle pressure around the knee joint by using three different sensors attached on the inner side of the knee brace (see Fig. 2(b)). For measuring the knee skin temperature, we used an NTC Thermistor whose resistance value changes with temperature. We applied a simple voltage divider rule to resolve thermistor's resistance value R , from the ADC value (10-bit) obtained from MetaWear CPro board acting as the data acquisition unit of the sensor (equation (16)).

$$R = \frac{R_B \times \text{ADC Reading}}{1023 - \text{ADC Reading}}. \quad (16)$$

The measured resistance R depends on the ADC reading, the bias resistor R_B in the voltage divider, and the ADC resolution (2^{10} in our system). The resistance was converted to temperature using the Steinhart–Hart equation or B (or β) parameter equation (equation (17)) which explains the resistance-temperature relationship of NTC thermistors [45].

$$\frac{1}{T} = \frac{1}{T_0} + \frac{1}{\beta} \ln \frac{R}{R_0}. \quad (17)$$

In equation (17), R is the thermistor's resistance at the skin temperature T , R_0 is the resistance at $T_0 = 25^\circ\text{C}$ (298 K) and β is a constant of the thermistor, and it is 3974 K for our sensor.

The working principle of the other two sensors, pressure and GSR, is the same as the temperature sensor – resistance variation with input stimulus. However, for these two sensors no bias resistors were added due to their higher ranges of resistance variation. In these cases, we first prepared a resistance (0 to 6 MΩ) vs ADC datasheet for this configuration (see Fig. 2(a)) and then used it to determine the resistance values of the sensors from the corresponding ADC readings. For the pressure sensor, we used the datasheet of FSR® 402 Short

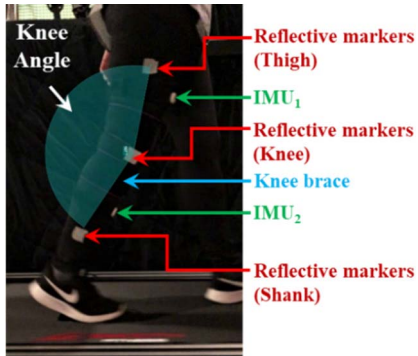


Fig. 7. Knee angle measurement validation.

to determine the corresponding pressure from the resistance value. Finally, we computed skin conductance G_{skin} , around the knee by inverting the resistance value R_{GSR} measured by the GSR sensor.

F. Energy Features

Joint motion signals, being complex, non-linear and non-stationary, and having variable spectral characteristics, can be effectively analyzed by decomposing them into their spectral components. To get the spectral components, we used wavelet packet decomposition (WPD) because of its fast and hierarchical tree-like decomposition algorithm, which makes it suitable for real-time applications [46]. WPD is a wavelet transform where the signal is passed through discrete-time low- and high-pass quadrature mirror filters to decompose the approximation coefficients and detail coefficients in the first level. Then, the following levels are calculated by passing both the detail and approximation coefficients from the previous level through similar low- and high-pass filters. Thus, the WPD allows the signal to decompose evenly throughout its whole spectrum. In our study, we used WPD at level 8 to decompose the preprocessed sensors' signals and calculated the energy information E of each decomposed signal using equation (18). Those energy features derived from the signal components are closely related with the mechanical work done during knee joint movements [15].

$$E = \frac{1}{M} \sum_{n=1}^N [S(n)]^2. \quad (18)$$

In equation (18), M represents the total number of gait cycles in the signal, N is the total number of samples and S denotes the decomposed signal components.

V. RESULTS AND DISCUSSION

A. Measurement Validation

1) Knee Angle: The complementary-filter based estimation of the knee joint angle was compared with Kalman filter-based estimation as it is considered as a superior tool for sensor fusion and widely used by many researchers for joint angle estimation from IMU sensors [47]–[50]. The estimations from both the complementary and Kalman filters showed similar results (Fig. 8), although the Kalman filtering-based approach requires significantly higher computational time (~120 times

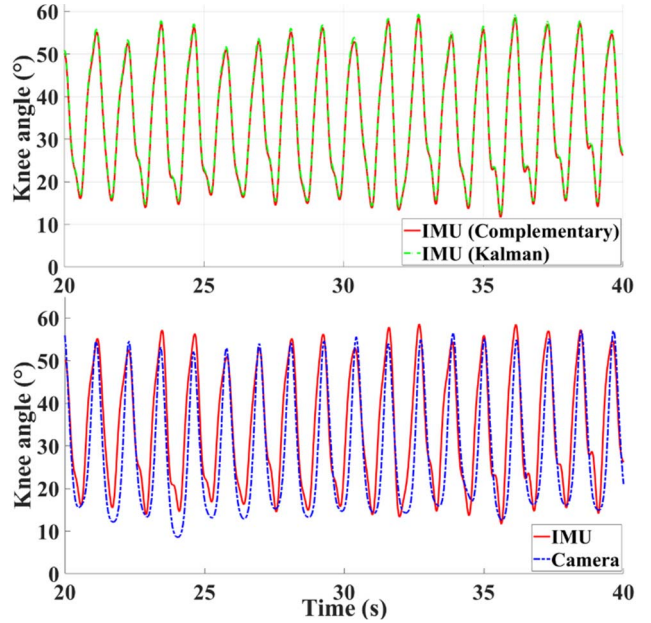


Fig. 8. Comparison of knee angle measurements.

more than the complementary filter-based approach) and larger processing memories due to its computational complexity. Therefore, we have chosen the complementary filtering method due to its simplicity, low computational requirements and comparable results.

For further validation, the results from our system were then compared to a video-based motion analysis system. Video-based systems are widely used to quantify joint kinematic data for human gait in a controlled environment [51]. We used a high-speed camera to capture two-dimensional (2D) videos of knee joint movements during walking on a treadmill and a freeware motion-analysis software Kinovea (version 0.8.26) [51] to analyze the video and quantify the knee joint angles during walking. Along with the knee monitoring system, three reflective markers were attached on specific lateral anatomical positions (thigh, knee and shank) of the subject's right lower limb as shown in Fig. 7. These markers are detected by the motion-analysis tool to quantify the joint angles during walking. We initialized both systems simultaneously to obtain synchronized data.

We used the concordance correlation coefficient ρ_C [33] to compare the knee angle measurements from both systems. This coefficient measures the agreement between two readings from the same sample by determining the variation from the concordance line (45° line through the origin). With this technique we can assess the reliability of a new algorithm or a device by comparing to another known technique. The calculation of ρ_C , comprises a measurement of precision ρ , and accuracy C_b , and is

$$\rho_C = \rho \times C_b. \quad (19)$$

Here, ρ is the Pearson correlation coefficient that measures how far each observation deviates from the best-fit line and it represents a measure of precision. C_b is a bias correction factor, which measures how far the best-fit line deviates from the 45° line through the origin and denotes a measure of

TABLE III
CONCORDANCE CORRELATION COEFFICIENT ρ_C
FOR WALKING TEST

ρ_C	0.9577
C_b	0.9820
ρ	0.9753

TABLE IV
MFC COMPARISON

	Avg. MFC from Video (mm)	Avg. MFC from IMU (mm)	Mean Error (mm)	(%)
Normal walk	19.86	20.07	0.21	1.1
Fast walk	26.21	27.40	1.19	4.5

accuracy. The value of ρ_C ranges from 0 (complete disagreement) to 1 (perfect concordance). The strength of agreement from the concordance correlation coefficient values is usually interpreted as “poor” (<0.90), “moderate” (0.90–0.95), “substantial” (0.95–0.99) and “almost perfect” (>0.99) [52]. The results obtained from the developed knee monitoring system showed substantial consistency ($\rho_C \cong 0.96$) with the readings from the video-based motion analysis system (Fig. 8 and Table III). In Fig. 8 it is also observed that the IMU measured knee angle showed small kinks in the lower part of the graph which are actually occurred when the feet hit the ground (generate vibrations) during walking. However, the video-based analysis system was unable to detect these small changes (vibrations) that can be noted as a limitation of the video-based system.

2) Stride Length, Gait Speed and Cadence: The proposed stride length, gait speed and cadence calculation algorithms were validated manually. In this method, the steps of the subjects were manually counted while performing the walking exercise and the total distance was measured using a measuring tape. Therefore, the average stride length was calculated using,

$$\text{Stride Length}_{\text{avg.}} = \frac{D}{\left(\frac{\text{number of steps}}{2}\right)}, \quad (20)$$

where D is the measured distance for walking exercise. As one stride consists of two consecutive steps, the total number of steps was divided by two to get the total number of strides. Time information (total duration T) of the walking exercise was retrieved from the IMU readings. Gait speed and cadence were then calculated using equations (21) and (22).

$$\text{Gait Speed} = \frac{D}{T}, \quad (21)$$

$$\text{Cadence} = \frac{\text{number of steps} \times 60}{T}. \quad (22)$$

This validation process included walking data from 10 subjects where we compared the results obtained from the proposed system with manually calculated values for stride length, gait speed and cadence. The walking distance for each subject was 65 meters straight. The highest estimation error for stride length was 4.81 cm (3.3%) and the mean error for 10 subjects was 2.48 cm (1.7%). Similarly, for gait speed, the highest estimation error was 3.8% (5.10 cm/s) and the mean error

was 2.1%. The cadence calculation using the knee monitoring system was also highly accurate with a mean error of 1.2%. Thus, these results proved the reliability of our system and algorithm for stride length, gait speed and cadence estimation.

3) Minimum Foot Clearance (MFC): We used the same video-based motion analysis system to validate the MFC measurement. In this case, one reflective marker was attached on the lateral side of the shoe to track the motion of the foot in the walking video. Then, we extracted the MFC (vertical distance between shoe sole and ground while the foot was parallel to the ground) from the tracked video to validate our measurement system. We measured MFC using both the systems simultaneously for normal and fast walking speed on the treadmill. In Table IV, a comparison between MFC calculations from the two systems is presented.

All the comparison results showed that the estimation of knee joint angle and gait parameters using our developed system were accurate and robust enough to be considered as a reliable device for knee joint and gait monitoring as well as assessment. We also collected multiple knee data from the same subjects walking under similar conditions but at different times and compared those data in order to ensure the reproducibility of the measurements using our system. For each case, the acquired data from all the sensors showed high consistency and small variations with the standard deviation of $\pm 7.5\%$ from the mean values.

B. Characteristics of Extracted Features

Typically, the bone density of a human body reaches its peak value around age 30, tends to remain stable with equal amounts of bone formation and bone breakdown from about age 30 to 50. After age of 50, bone breakdown starts to exceed bone formation, resulting in bone loss and joint health degradation [53], [54]. Therefore, we divided the subjects in our study into three age groups (18–30, 31–50 and 51–86 years) to compare their knee joint features ($p < 0.05$). Each of these groups was also divided according to their gender to show the comparison between male and female subjects of same age groups (Fig. 9 and Table V).

Although all subjects were healthy and performed their walking experiments for joint monitoring at their preferred pace and comfort, we found variations in the characteristics for several extracted features among different subject groups. On average, the female subjects in our study walked with a higher knee angle change (50.2°) compared to the male subjects (48.2°) (Table V). A higher knee angle change involves higher angular movements (flexion, extension) of knee joints within its range, thus causing increased generation or absorption of joint power [55]. Also, when we compared thigh and shank angle changes during walking (Fig. 9 and Table V), the female subjects exhibited higher thigh angle change (33.9°) than the male subjects (31.5°) due to their greater pelvic tilt and larger hip swing while walking [56]. Compared to male pelvis, the structure of the female pelvis, commonly referred to as gynecoid pelvis, is distinctly different, with a wider sacrum and pubic arch. This anatomical difference coupled with a relatively lax ligament of the female pelvis and hip joints results in a larger hip swing and thigh

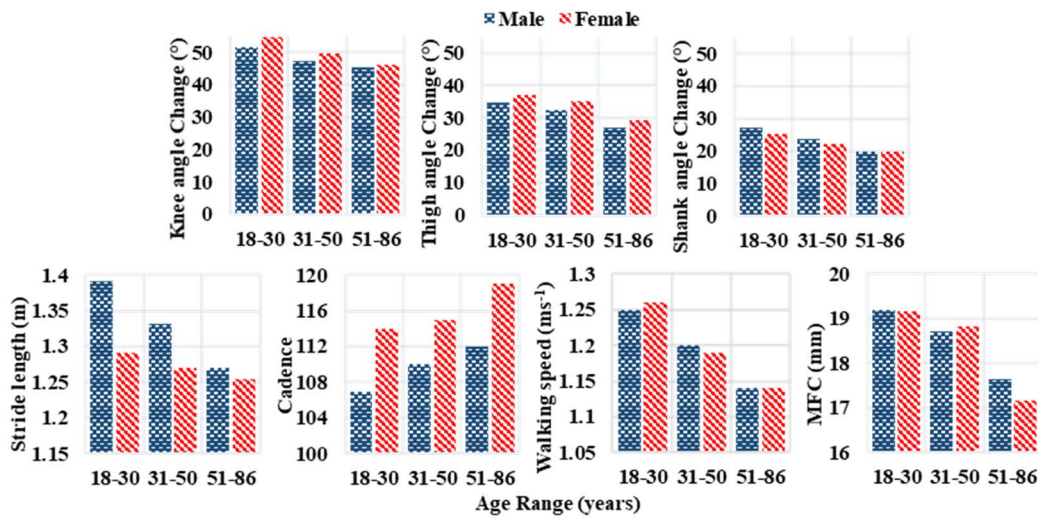


Fig. 9. Comparison of magnitude of different knee joint and gait-related parameters.

TABLE V
ANGLES, STRIDE LENGTH, CADENCE, SPEED AND MFC OF WALKING

Age	Knee Angle Change (°)			Thigh Angle Change (°)			Shank Angle Change (°)			Stride Length (m)			Cadence			Walking Speed (ms⁻¹)			MFC (mm)		
	Male	Female	Avg.	Male	Female	Avg.	Male	Female	Avg.	Male	Female	Avg.	Male	Female	Avg.	Male	Female	Avg.	Male	Female	Avg.
18-30	51.8	54.6	53.2	34.7	37.1	35.9	27.1	25.4	26.2	1.39	1.29	1.34	107	114	111	1.25	1.26	1.26	19.19	19.18	19.19
31-50	47.5	49.7	48.6	32.5	35.2	33.9	23.6	22.2	22.9	1.33	1.27	1.30	110	115	113	1.20	1.19	1.20	18.71	18.83	18.77
51-86	45.2	46.2	45.7	27.2	29.5	28.3	20.0	19.8	19.9	1.27	1.25	1.26	112	119	116	1.14	1.14	1.14	17.66	17.17	17.41
Avg.	48.2	50.2	49.2	31.5	33.9	33.2	23.6	22.5	23.1	1.33	1.27	1.29	110	116	113	1.20	1.20	1.20	18.52	18.39	18.50

movement among the females. On the contrary, the male subjects showed larger shank angle change (23.6°) than females (22.5°) (Table V).

It was also observed that the average magnitude of overall knee angle changes, as well as thigh and shank angle changes, declined for the subjects in the older age range (Fig. 9). This is because with aging, joint movement becomes stiffer and less flexible due to a gradual reduction of the lubricating fluid inside the knee joints and the cartilage becomes thinner. Also, the ligaments tend to shorten and lose some flexibility, restricting joint movements [57].

We also compared different gait characteristics (average values) measured with our knee monitoring system and found them to be distinctly different among the three groups (Table V and Fig. 9). It was observed that the female subjects had shorter stride length (1.27 m) and a higher cadence (116 steps/min) during walking, while the male subjects walked with longer stride length (1.33 m) and a lower cadence (110 steps/min) (Table V). A higher cadence and shorter stride length usually require increased joint torque and power during walking [58], thus showing a tendency among the females to expend more energy while walking.

Similarly, subjects from the older age group (51-86) walked with shorter stride length (1.26 m) and a higher cadence (116 steps/min) compared to the younger adults (Table V). The gradual deterioration of joint health with aging affects balance and stability among the older adults and they tend to compensate for these issues by decreasing their stride length and increasing their cadence. It was also observed that the older subjects walked with a slower gait speed compared to the younger subjects (Fig. 9) and decreased speed is associated

with the risk of adverse health-related outcomes [59]. The reduced stride length, gait speed and knee joint movement among older adults also affect their MFC while walking. As a result, adults in the “51-86” age range in our study showed the lowest average MFC (17.4 mm) among the three age groups (Table V). MFC is a key gait cycle parameter for predicting the likelihood of a trip or fall. It occurs during the mid-swing phase in a walking cycle where the forward velocity of the foot is maximum. Thus, a high forward velocity coupled with a low MFC increases the possibility of unanticipated foot-ground contacts, resulting in trips and falls during walking [43]. Therefore, our knee monitoring system can potentially be used for continuous monitoring and analyzing of an individual’s gait characteristics to identify the unsteady gait as well as to predict the possibility of trips and falls when the MFC is very low.

We also calculated and compared the energies of the significant components ($p < 0.009$) of the decomposed signals from the accelerometer and gyroscope data for all three axes (Fig. 10 and Table VI). It was observed that the average energies of the mediolateral (y-axis) and anteroposterior (z-axis) acceleration were significantly higher for female subjects than the male subjects (Fig. 10). As discussed earlier, females tend to have larger hip and knee flexion as well as higher mediolateral movement which causes higher power absorption during the gait cycle. Moreover, as females walk with a higher cadence and shorter stride length compared to males [15], their knee joints and adjacent muscles need to perform higher amounts of mechanical work than males during walking for a fixed distance in the same time. The female subjects also exhibited higher rotational energy around the mediolateral (y-axis), longitudinal (x-axis) and anteroposterior (z-axis)

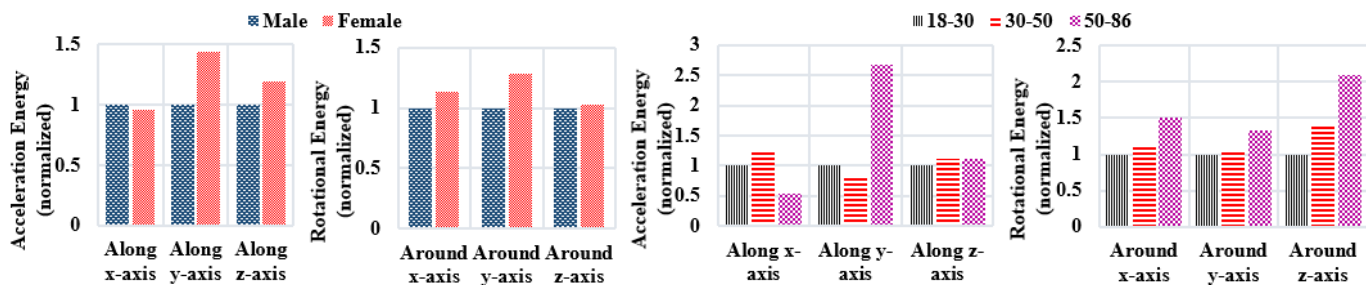


Fig. 10. Comparison of acceleration and rotational energy between different subject groups.

TABLE VI
ACCELERATION AND ROTATIONAL ENERGY

Age	Gyroscope									Accelerometer								
	Around x-axis*			Around y-axis*			Around z-axis*			Along x-axis			Along y-axis			Along z-axis		
	Male	Female	Avg.	Male	Female	Avg.	Male	Female	Avg.	Male	Female	Avg.	Male	Female	Avg.	Male	Female	Avg.
18-30	50.37	50.97	50.67	170.96	212.79	191.88	18.88	10.47	14.67	123.45	106.98	115.21	29.13	42.05	35.59	38.17	44.31	41.24
31-50	52.46	62.58	57.52	178.03	222.74	200.39	16.18	26.31	21.25	139.71	143.32	141.51	20.46	38.76	29.61	41.41	48.81	45.11
51-86	69.95	83.86	76.90	224.22	286.17	255.20	29.96	30.05	30.01	63.39	61.59	62.49	85.17	105.16	95.17	40.44	48.50	44.47
Avg.	57.59	65.80		191.07	240.57		21.67	22.28		108.85	103.96		44.92	61.99		40.00	47.21	

* Energy values of the gyroscope correspond to the value multiplied by 10^4 .

directions compared to their male counterparts. The distinct higher magnitudes of mediolateral (y-axis) acceleration energy, and rotational energy around mediolateral (y-axis) and longitudinal (x-axis) axes of females (Fig. 10) represent their larger hip and knee joint movements while walking.

A significantly higher average (270%-320%) of mediolateral (y-axis) acceleration energy and a lower average (45%-55%) of longitudinal (x-axis) acceleration energy among the older (51-86) age group can be attributed to their reduced balance and stability while walking [15] (Table VI). Their postural balance and alignment are affected due to larger mediolateral sway and lower longitudinal movements (low foot clearance). In addition, higher rotational energy around all three axes in older adults (Table VI) could be attributed to their increased asymmetry and variability in gait [15]. Generally, the younger adults possess better musculoskeletal health and an unimpaired somatosensory system. Therefore, their basal energy expenditure remains well controlled with better postural balance and alignment, as well as superior motor-cognitive coordination [60]. In summary, a significant decline in knee joint angle, balance and gait symmetry among older age groups demonstrates an overall deterioration of knee joint health along with vulnerable gait compared to the younger age groups.

In our study, we also analyzed the pressure change of the anterior compartment muscles (quadriceps) of the thigh (directly connected with knee patella) while walking and made a comparison between different gender and age groups (Fig. 11 and Table VII). It was observed that the male subjects exhibited stronger muscle pressure in comparison with the female subjects. Usually, males tend to have larger thigh muscle mass than females. Also, male muscles are more solid, due to having a higher proportion of Type 2 fast-twitch fibers [61]. This kind of muscle fiber contains a lot of protein but less amount of blood. It has the ability to expand and contract rapidly with great force and generate its own energy. As men have about 50% more Type 2 muscle fibers than women's, they

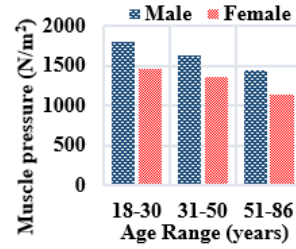


Fig. 11. Comparison of thigh muscle pressure between different subject groups.

TABLE VII
THIGH ANTERIOR COMPARTMENT MUSCLE
PRESSURE WHILE WALKING

Age	Muscle Pressure (N/m ²)		
	Male	Female	Avg.
18-30	1802	1460	1631
31-50	1637	1359	1498
51-86	1439	1136	1287
Avg.	1626	1318	

produce more pressure while walking [61]. It is also known that muscle mass and volume among older adults decrease gradually with age [62]. As a result, the force generated due to muscle expansion and contraction begins to decline which signifies the deterioration of musculoskeletal health among older adults. In our experiments, we also found that the older (51-86) age group had the lowest thigh muscle pressure in comparison with the younger people during walking.

Using our system, we also measured local knee skin temperature and skin conductance during walking experiments. Usually, changes in knee skin temperature occur due to the changes in blood flow in that region and this change can be an indication of abnormality. For example, the skin temperature of an inflamed knee is usually higher ($1.09\text{ }^\circ\text{C}$ – $2.77\text{ }^\circ\text{C}$) than a normal knee ($\sim 30.6\text{ }^\circ\text{C}$ on average) [63], [64]. Similarly, stress and perspiration in the knee joints are related to the

local blood flow and the sweat gland activities which vary due to external and internal stimuli. These variations can be assessed by measuring the changes in the skin conductance. However, for both these cases, long-time monitoring is needed to detect any noticeable changes. Therefore, in our current study, we could not distinguish these kinds of variation as all participants were clinically healthy and we only collected each knee data for a short period of time. Instead, we have calculated the average value from our collected data for normal knee skin temperature which was 30.26°C with a standard deviation of 0.93°C . We also performed dry (normal) and wet knee (after workout) skin conductance measurement tests for two participants where the average conductance for dry skin was $38\ \mu\text{S}$ and $46\ \mu\text{S}$ for wet skin. In every measurement, the two GSR electrodes and the temperature sensor were placed on the knee patella (Fig. 2(b)) for better skin contact. The gap between two GSR electrodes was 6 cm (side by side).

VI. CONCLUSION AND FUTURE WORK

Longer life expectancies and increased incidence of obesity are placing an increased demand on load-bearing joints. Among all the load-bearing joints, the knee joint is considered as the most important and critical for health assessment due to its huge amount of pressure absorption with every lower limb activity and high exposure to injuries. A simple, easy-to-use and low-cost yet reliable knee monitoring system would therefore be of immense benefit for remote monitoring of the knee joint health status of elderly people as well as the people undergoing rehabilitation, thus facilitating healthy joints at home.

In this research, we developed a multi-sensor-based non-invasive, comfortable, wearable and easy-to-use knee joint monitoring device, which can be used continuously without hindering persons' day-to-day activities. The system is composed of inertial motion, temperature, pressure and skin conductance sensors which allow it to simultaneously measure knee movements as well as other physiological parameters such as skin temperature, conductance and muscle pressure around the knee joint. These parameters can potentially be used by the medical experts to determine the overall knee joint health and mobility status of an individual. Thus, the smart wearable knee monitoring system can be used for early diagnoses of joint disorders such as osteoarthritis and osteoporosis, fall detection, and post-surgery monitoring of patient's mobility and rehabilitation. However, to make the knee joint monitoring system more precise and efficient, we plan to address several important research topics in our future work.

First, this work only included healthy subjects who were supposed to possess comparably better joint functionalities and gait than the people with known joint disorders. The knee joint functionalities and movement pattern change gradually through different disease processes and at different severities, thus its characteristics is likely to deviate from those of healthy joints corresponding to an individual's peer group. Even though distinct variations in the characteristics among different subject groups are reported in this work, further in-depth study on a larger balanced dataset including subjects having different knee joint-related issues or diagnosed diseases

with a wider range of age and BMI would be beneficial to reinforce our inferences.

Second, this research involves human subjects and their health information, so it is mandatory to fulfill all the requirements set by the responsible regulatory bodies such as data privacy, security and other ethical conditions. Therefore, before it can be used on patients, an additional approval from our University's Research Ethics Board (REB) is required demonstrating the system's feasibility and reliability.

Third, in this study, we mainly focused on the straight plane surface walking of an individual to keep the analysis model simple and evaluate its feasibility. In the next step, we will include a diverse database based on walking signals from different surfaces, different conditions, different footwear, and more varied daily lower limb activities at home and in a community environment to reinforce our analysis and findings. We also hope to introduce a health index for knee joints based on the extracted key features that can act as a baseline to distinguish atypical knee joint characteristics from normal knee joints for different groups and activities. This index can be used as reference by medical practitioners and even by individuals to quickly determine the knee health condition.

Fourth, in this research, we measured a single knee joint at a time which limits the asymmetry and variability analysis between two knee joints' characteristics while walking. These kinds of analyses are required to determine the degree of coordination between two knees as well as lower limb dominance. Hence, we plan to use two systems on two legs that will allow us to collect simultaneous data from both the knee joints during walking and other lower limb activities.

Fifth, we will also work towards developing a stand-alone smart program integrated with a combined data acquisition, analysis and modeling techniques for further feedback and prediction application. Cloud server communication will also be set up for real-time data mining and handling large data using proper algorithms. Thus, we will be able to exploit the knee monitoring system for early diagnoses of joint disorders, real-time fall detection and prevention, athletes' performance evaluation and rehabilitation progress.

Sixth, the developed knee monitoring system can be used to evaluate knee joint health and also to extract several gait features that prove its feasibility as a gait analyzer. Since gait is correlated with human cognitive and cardiovascular activities, it is possible to utilize these extracted gait features to find a quantitative correlation with cognitive and cardiovascular functions. This correlation can potentially be exploited in predicting the development of neurodegenerative disorders (e.g., dementia, Alzheimer's, Parkinson's, etc.) and diseases associated with cardiovascular systems.

Finally, our ultimate goal is to develop an accurate, easy-to-use, low-cost, non-invasive wearable smart joint monitoring and assistive system coupled with the internet of things (IoT) to facilitate remote long-term joint health monitoring and real-time assessment. This smart system, taking advantage of the IoT, would also be able to provide important joint-related information to medical professionals for early and accurate diagnosis of joint-related problems and diseases as well as more efficient and effective medical intervention when needed.

REFERENCES

- [1] *Seniors Care | CMA Health Topics*. Accessed: Sep. 5, 2019. [Online]. Available: <https://www.cma.ca/seniors-care>
- [2] *Mobility in Aging—A Strategic Initiative of the CIHR Institute of Aging—CIHR*. Accessed: Sep. 5, 2019. [Online]. Available: <http://www.cihr-irsc.gc.ca/e/29994.html#3>
- [3] A. S. Fahy *et al.*, “A review of hip fracture mortality—Why and how does such a large proportion of these elderly patients die?” *Surgical Sci.*, vol. 05, no. 5, pp. 227–232, 2014.
- [4] M. J. Deen, “Information and communications technologies for elderly ubiquitous healthcare in a smart home,” *Pers. Ubiquitous Comput.*, vol. 19, nos. 3–4, pp. 573–599, Jul. 2015.
- [5] S. Majumder and M. J. Deen, “Smartphone sensors for health monitoring and diagnosis,” *Sensors*, vol. 19, no. 9, p. 2164, May 2019.
- [6] L. Bornhöft, J. Thorn, M. Svensson, L. Nordeman, R. Eggertsen, and M. E. H. Larsson, “More cost-effective management of patients with musculoskeletal disorders in primary care after direct triaging to physiotherapists for initial assessment compared to initial general practitioner assessment,” *BMC Musculoskeletal Disorders*, vol. 20, no. 1, p. 186, Dec. 2019.
- [7] K. Nisar, A. A. A. Ibrahim, L. Wu, A. Adamov, and M. J. Deen, “Smart home for elderly living using wireless sensor networks and an Android application,” in *Proc. IEEE 10th Int. Conf. Appl. Inf. Commun. Technol. (AICT)*, Oct. 2016, pp. 1–8.
- [8] S. Majumder *et al.*, “Smart homes for elderly healthcare—Recent advances and research challenges,” *Sensors*, vol. 17, no. 11, p. 2496, Oct. 2017.
- [9] Y. Liu *et al.*, “A novel cloud-based framework for the elderly healthcare services using digital twin,” *IEEE Access*, vol. 7, pp. 49088–49101, 2019.
- [10] M. A. H. M. Adib and M. F. Jaafar, “Modelling of meniscus of knee joint during soccer kicking,” in *Proc. IOP Conf., Mater. Sci. Eng.*, Dec. 2013, vol. 50, no. 1, Art. no. 012027.
- [11] *Why Weight Matters When it Comes to Joint Pain—Harvard Health*. Accessed: Mar. 8, 2020. [Online]. Available: <https://www.health.harvard.edu/pain/why-weight-matters-when-it-comes-to-joint-pain>
- [12] A. I. Faisal, S. Majumder, T. Mondal, D. Cowan, S. Naseh, and M. J. Deen, “Monitoring methods of human body joints: State-of-the-art and research challenges,” *Sensors*, vol. 19, no. 11, p. 2629, Jun. 2019.
- [13] B. Jin *et al.*, “Walking-age analyzer for healthcare applications,” *IEEE J. Biomed. Health Informat.*, vol. 18, no. 3, pp. 1034–1042, May 2014.
- [14] P. Mandal, K. Tank, T. Mondal, C.-H. Chen, and M. J. Deen, “Predictive walking-age health analyzer,” *IEEE J. Biomed. Health Informat.*, vol. 22, no. 2, pp. 363–374, Mar. 2018.
- [15] S. Majumder, T. Mondal, and M. J. Deen, “A simple, low-cost and efficient gait analyzer for wearable healthcare applications,” *IEEE Sensors J.*, vol. 19, no. 6, pp. 2320–2329, Mar. 2019.
- [16] S. Majumder, T. Mondal, and M. Deen, “Wearable sensors for remote health monitoring,” *Sensors*, vol. 17, no. 12, p. 130, Jan. 2017.
- [17] K. Nisar and A. A. A. Ibrahim, “A model new for smart home technologies knee monitor and walking analyser,” in *Advances in Intelligent Systems and Computing*. Singapore: Springer, 2018, pp. 501–509.
- [18] V. M. Pomeroy, E. Evans, and J. D. Richards, “Agreement between an electrogoniometer and motion analysis system measuring angular velocity of the knee during walking after stroke,” *Physiotherapy*, vol. 92, no. 3, pp. 159–165, Sep. 2006.
- [19] P. Piriyaprasarth, M. E. Morris, A. Winter, and A. E. Bialocerkowski, “The reliability of knee joint position testing using electrogoniometry,” *BMC Musculoskeletal Disorders*, vol. 9, no. 1, Dec. 2008.
- [20] K. Rome and F. Cowieson, “A reliability study of the universal goniometer, fluid goniometer, and electrogoniometer for the measurement of ankle dorsiflexion,” *Foot Ankle Int.*, vol. 17, no. 1, pp. 28–32, Jan. 1996.
- [21] L. Tesio, M. Monzani, R. Gatti, and F. Franchignoni, “Flexible electrogoniometers: Kinesiological advantages with respect to potentiometric goniometers,” *Clin. Biomech.*, vol. 10, no. 5, pp. 275–277, Jul. 1995.
- [22] A. Mobini, S. Behzadipour, and M. S. Foumani, “Accuracy of Kinect’s skeleton tracking for upper body rehabilitation applications,” *Disabil. Rehabil.: Assistive Technol.*, vol. 9, no. 4, pp. 344–352, Jul. 2014.
- [23] Z. Wang, G. Liu, and G. Tian, “Human skeleton tracking using information weighted consensus filter in distributed camera networks,” in *Proc. Chin. Autom. Congr. (CAC)*, Oct. 2017, pp. 4640–4644.
- [24] M. U. Islam, H. Mahmud, F. B. Ashraf, I. Hossain, and M. K. Hasan, “Yoga posture recognition by detecting human joint points in real time using microsoft kinect,” in *Proc. IEEE Region 10 Humanitarian Technol. Conf. (R10-HTC)*, Dec. 2017, pp. 668–673.
- [25] D. Z. Stupar, J. S. Bajic, L. M. Manojlovic, M. P. Slankamenac, A. V. Joza, and M. B. Zivanov, “Wearable low-cost system for human joint movements monitoring based on fiber-optic curvature sensor,” *IEEE Sensors J.*, vol. 12, no. 12, pp. 3424–3431, Dec. 2012.
- [26] M. Donno, E. Palange, F. Di Nicola, G. Bucci, and F. Ciancetta, “A new flexible optical fiber goniometer for dynamic angular measurements: Application to human joint movement monitoring,” *IEEE Trans. Instrum. Meas.*, vol. 57, no. 8, pp. 1614–1620, Aug. 2008.
- [27] C. K. Lim, Z. Luo, I.-M. Chen, and S. H. Yeo, “A low cost wearable optical-based goniometer for human joint monitoring,” *Frontiers Mech. Eng. China*, pp. 13–22, Dec. 2010.
- [28] P. T. Gibbs and H. H. Asada, “Wearable conductive fiber sensors for multi-axis human joint angle measurements,” *J. Neuroeng. Rehabil.*, vol. 2, no. 1, p. 7, 2005.
- [29] J. H. M. Bergmann, S. Anastasova-Ivanova, I. Spulber, V. Gulati, P. Georgiou, and A. McGregor, “An attachable clothing sensor system for measuring knee joint angles,” *IEEE Sensors J.*, vol. 13, no. 10, pp. 4090–4097, Oct. 2013.
- [30] G. Gioberto, “Garment-integrated wearable sensing for knee joint monitoring,” in *Proc. ACM Int. Symp. Wearable Comput. Adjunct Program (ISWC Adjunct)*, 2014, pp. 113–118.
- [31] S. Park *et al.*, “Highly bendable and rotational textile structure with prestrained conductive sewing pattern for human joint monitoring,” *Adv. Funct. Mater.*, vol. 29, no. 10, Mar. 2019, Art. no. 1808369.
- [32] Y. Zheng *et al.*, “A highly stretchable and stable strain sensor based on hybrid carbon nanofillers/polydimethylsiloxane conductive composites for large human motions monitoring,” *Composites Sci. Technol.*, vol. 156, pp. 276–286, Mar. 2018.
- [33] J. J. Castañeda, A. F. Ruiz-Olaya, C. N. Lara-Herrera, and F. Z. Roldán, “Knee joint angle monitoring system based on inertial measurement units for human gait analysis,” in *Proc. IFMBE*, vol. 60, I. Torres, J. Bustamante, and D. A. Sierra, Eds. Singapore: Springer, 2017, pp. 690–693.
- [34] P. N. Pathirana, M. S. Karunaratne, G. L. Williams, P. T. Nam, and H. Durrant-Whyte, “Robust and accurate capture of human joint pose using an inertial sensor,” *IEEE J. Translational Eng. Health Med.*, vol. 6, pp. 1–11, 2018.
- [35] T. Seel, J. Raisch, and T. Schauer, “IMU-based joint angle measurement for gait analysis,” *Sensors*, vol. 14, no. 4, pp. 6891–6909, Apr. 2014.
- [36] S. Bakhshi, M. H. Mahoor, and B. S. Davidson, “Development of a body joint angle measurement system using IMU sensors,” in *Proc. Annu. Int. Conf. IEEE Eng. Med. Biol. Soc.*, Aug. 2011, pp. 6923–6926.
- [37] C. N. Teague *et al.*, “Novel methods for sensing acoustical emissions from the knee for wearable joint health assessment,” *IEEE Trans. Biomed. Eng.*, vol. 63, no. 8, pp. 1581–1590, Aug. 2016.
- [38] J. M. Soucie *et al.*, “Range of motion measurements: Reference values and a database for comparison studies,” *Haemophilia*, vol. 17, no. 3, pp. 500–507, May 2011.
- [39] O. O. Akintade and L. O. Kehinde, “Comparison of data fusion techniques for human knee joint range-of-motion measurement using inertial sensors,” *Int. J. Electron. Electr. Eng.*, vol. 5, no. 2, pp. 127–134, 2017.
- [40] Q. Li, M. Young, V. Naing, and J. M. Donelan, “Walking speed estimation using a shank-mounted inertial measurement unit,” *J. Biomech.*, vol. 43, no. 8, pp. 1640–1643, May 2010.
- [41] F. Dadashi, B. Mariani, S. Rochat, C. Büla, B. Santos-Eggimann, and K. Aminian, “Gait and foot clearance parameters obtained using shoe-worn inertial sensors in a large-population sample of older adults,” *Sensors*, vol. 14, no. 1, pp. 443–457, Dec. 2013.
- [42] Y. Wahab, A. Zayegh, R. K. Begg, and R. Veljanovski, “Analysis of foot-to-ground clearance measurement techniques for MEMS realization,” in *Proc. 10th Int. Conf. Comput. Inf. Technol.*, Dec. 2007, pp. 1–5.
- [43] R. Begg, R. Best, L. Dell’Oro, and S. Taylor, “Minimum foot clearance during walking: Strategies for the minimisation of trip-related falls,” *Gait Posture*, vol. 25, no. 2, pp. 191–198, Feb. 2007.
- [44] *Step Length, Cadence, and the Walk Ratio?* ProtoKinetics. Accessed: Feb. 20, 2020. [Online]. Available: <https://www.protokinetics.com/2018/10/17/step-length-cadence-and-the-walk-ratio/>
- [45] C. Chen, “Evaluation of resistance–temperature calibration equations for NTC thermistors,” *Measurement*, vol. 42, no. 7, pp. 1103–1111, Aug. 2009.
- [46] V. Krishnan and B. Anto, “Features of wavelet packet decomposition and discrete wavelet transform for malayalam speech recognition,” *Int. J. Recent Trends Eng.*, vol. 1, no. 2, pp. 93–96, 2009.
- [47] M. El-Gohary, S. Pearson, and J. McNames, “Joint angle tracking with inertial sensors,” in *Proc. 30th Annu. Int. Conf. IEEE Eng. Med. Biol. Soc.*, Aug. 2008, pp. 1068–1071.
- [48] X. Yun and E. R. Bachmann, “Design, implementation, and experimental results of a quaternion-based Kalman filter for human body motion tracking,” *IEEE Trans. Robot.*, vol. 22, no. 6, pp. 1216–1227, Dec. 2006.
- [49] G. F. Welch, “HISTORY: The use of the kalman filter for human motion tracking in virtual reality,” *Presence: Teleoperators Virtual Environ.*, vol. 18, no. 1, pp. 72–91, Feb. 2009.

- [50] S. B. Sudin, "Wireless knee joint angle measurement system using gyroscope," M.S. thesis, Dept. Elect. Electron. Eng., Univ. Tun Hussein Onn Malaysia, Parit Raja, Malaysia, 2012.
- [51] C. Damsted, R. O. Nielsen, and L. H. Larsen, "Reliability of video-based quantification of the knee-and hip angle at foot strike during running," *Int. J. Sports Phys. Therapy*, vol. 10, no. 2, pp. 147–154, Apr. 2015.
- [52] G. McBride, J. M. Bland, D. G. Altman, and L. I. Lin, "A proposal for strength-of-agreement criteria for Lin's concordance correlation coefficient," NIWA, Hamilton, New Zealand, NIWA Client Rep. HAM2005-062, 2005.
- [53] *Osteoporosis: What You Need to Know as You Age | Johns Hopkins Medicine*. Accessed: Feb. 20, 2020. [Online]. Available: <https://www.hopkinsmedicine.org/health/conditions-and-diseases/osteoporosis/osteoporosis-what-you-need-to-know-as-you-age>
- [54] *How to Feed Your Bones and Increase Bone Density—UBMD Orthopaedics & Sports Medicine Doctors—Buffalo*, Niagara Falls, New York. Accessed: Feb. 20, 2020. [Online]. Available: <https://ubortho.com/news/feed-bones-increase-bone-density/>
- [55] D. A. Winter, "Energy generation and absorption at the ankle and knee during fast, natural, and slow cadences," *Clin. Orthopaedics Rel. Res.*, vol. 175, pp. 147–154, May 1983.
- [56] K. M. T. Goutier, S. L. Jansen, C. G. C. Horlings, U. M. Kung, and J. H. J. Allum, "The influence of walking speed and gender on trunk sway for the healthy young and older adults," *Age Ageing*, vol. 39, no. 5, pp. 647–650, Sep. 2010.
- [57] *Ageing—Muscles Bones and Joints—Better Health Channel*. Accessed: Jan. 2, 2020. [Online]. Available: <https://www.betterhealth.vic.gov.au/health/conditionsand treatments/ageing-muscles-bones-and-joints>
- [58] L. Lee and W. E. L. Grimson, "Gait analysis for recognition and classification," in *Proc. 5th IEEE Int. Conf. Autom. Face Gesture Recognit.*, May 2002, pp. 155–162.
- [59] T. D. A. Busch *et al.*, "Factors associated with lower gait speed among the elderly living in a developing country: A cross-sectional population-based study," *BMC Geriatrics*, vol. 15, no. 1, p. 35, Dec. 2015.
- [60] H. Shimokata and F. Kuzuya, "Aging, basal metabolic rate, and nutrition," *Nihon Ronen Igakkai zasshi. Jpn. J. Geriatrics*, vol. 30, no. 7, pp. 572–576, 1993.
- [61] S. Nuell *et al.*, "Sex differences in thigh muscle volumes, sprint performance and mechanical properties in national-level sprinters," *PLoS ONE*, vol. 14, no. 11, Nov. 2019, Art. no. e0224862.
- [62] R. McCormick and A. Vasilaki, "Age-related changes in skeletal muscle: Changes to life-style as a therapy," *Biogerontology*, vol. 19, no. 6, pp. 519–536, Dec. 2018.
- [63] H. A. Ménard and D. Paquette, "Skin temperature of the knee: An unrecognized physical sign of inflammatory disease of the knee," *Can. Med. Assoc. J.*, vol. 122, no. 4, pp. 439–440, Feb. 1980.
- [64] K. Ammer, "Temperature of the human knee—A review," *Thermol. Int.*, vol. 12, pp. 137–151, 2012.



Abu Ilius Faisal received the B.Sc. degree in electrical and electronic engineering from the Islamic University of Technology, Gazipur, Bangladesh, and the M.A.Sc. degree in electrical and computer engineering from McMaster University, Hamilton, Canada, in 2009 and 2020, respectively, where he is currently pursuing the Ph.D. degree in electrical and computer engineering. His research interests include wearable sensors and devices, biomedical signal processing, machine learning, and pattern recognition.



Sumit Majumder (Graduate Student Member, IEEE) received the B.Sc. degree in electrical and electronic engineering from the Bangladesh University of Engineering and Technology, Dhaka, Bangladesh, and the M.A.Sc. degree in electrical and computer engineering from McMaster University, Hamilton, Canada, in 2007 and 2011, respectively, where he is currently pursuing the Ph.D. degree in electrical and computer engineering. His research interests include wearable sensors, biomedical signal processing, machine learning, and pattern recognition.



Ryan Scott received the B.Eng. degree in electrical engineering from McMaster University, Hamilton, ON, Canada, in 2019, where he is currently pursuing the M.A.Sc. degree in electrical engineering. His current research interests include high-performance CMOS time-to-digital converters and SPADs for biomedical imaging applications.



Tapas Mondal has been a Pediatric Cardiologist at McMaster University since 2005. He is an Associate Professor of Pediatrics with McMaster University and an Associate Member with the Hospital for Sick Children, Toronto, and also an Associate Member with the Faculty of Engineering, McMaster University. Dr. Mondal was honored with the Best Teacher award from McMaster University in 2009 (also nominated as Best teacher in 2006 and 2020) and also received the Best Senior Resident honor from Kalawati Saran Children's Hospital in New Delhi, India. He was awarded Jeffrey Coates award in 2018 as the first Pediatrician recipient considered to be the best physician of the city of Hamilton. He delivers integrated, personalized, family-centered patient care while creating an advanced learning environment for highly skilled personnel. His research interests center around different imaging techniques including low-cost health monitoring systems.



David Cowan received the B.A. (Hons.) degree in economics and the master's degree in industrial relations from Queen's University, Kingston, ON, Canada, in 1985 and 1987, respectively and the M.D. degree. He completed the Internal Medicine Fellowship and the Geriatric Medicine Fellowship at the McMaster Medical School, in 1996 and 1997, respectively. He is an Associate Professor with the Division of Geriatric Medicine, Department of Medicine, McMaster University, and a Consultant at St. Joseph's Healthcare and Hamilton Health Sciences, Hamilton, ON, Canada. His research interests include perioperative care of the elderly, diagnosis of Alzheimer's disease, gait assessment, and cognitive testing. He is a Fellow of RCPC.



M. Jamal Deen (Life Fellow, IEEE) is a Distinguished University Professor, a Senior Canada Research Chair of Information Technology, and the Director of the Micro- and Nano-Systems Laboratory, McMaster University. He served as the elected President of the Academy of Science, The Royal Society of Canada from 2015 to 2017. His current research interests are nanoelectronics, optoelectronics, nanotechnology, data analytics and their emerging applications to health and environmental sciences. Dr. Deen's research record includes more than 600 peer-reviewed articles (about 20% are invited), two textbooks on "Silicon Photonics- Fundamentals and Devices" and "Fiber Optic Communications: Fundamentals and Applications". His awards and honors include the Callinan Award as well as the Electronics and Photonics Award from the Electrochemical Society; a Humboldt Research Award from the Alexander von Humboldt Foundation; the Eadie Medal from the Royal Society of Canada; McNaughton Gold Medal (highest award for engineers), the Fessenden Medal and the Ham Education Medal (highest award for educators), all from IEEE Canada IEEE Canada. In addition, he was awarded the four honorary doctorate degrees in recognition of his exceptional research and scholarly accomplishments, exemplary professionalism and valued services. He has also been an elected Fellow status in 12 national academies and professional societies including The Royal Society of Canada, the Canadian Academy of Engineering, Chinese Academy of Sciences, and American Physical Society and Electrochemical Society). Recently, he was elected to the Order of Canada (July 2018), the highest civilian honor awarded by the Government of Canada.